Physica Medica 62 (2019) 13–19

Contents lists available at ScienceDirect

Physica Medica

journal homepage: www.elsevier.com/locate/ejmp

Original paper

Monte carlo study of organ doses and related risk for cancer in Tanzania from scattered photons in cervical radiation treatment involving Co-60 source

Suleiman Ameir Suleiman[a,b,*], Yaping Qi[a], Zhi Chen[a], X. George Xu[a,c]

[a] Department of Engineering and Applied Physics, School of Physical Sciences, University of Science and Technology of China, Hefei, Anhui Province 230027, PR China
[b] Ionizing Radiation Department, Tanzania Atomic Energy Commission, 23114 Block J Njiro, PO BOX 743, Arusha, United Republic of Tanzania
[c] Nuclear Engineering Program, Rensselaer Polytechnic Institute, Troy, NY 12180, USA

ARTICLE INFO

Keywords:
Monte Carlo simulation
Secondary cancer risk
Radiotherapy
Cervical cancer

ABSTRACT

Purpose: The present work aimed to evaluate organ doses and related risk for cancer from external beam radiation treatment (EBRT) and high-dose-rate (HDR) brachytherapy (BT) involving Co-60 source for patients with cervical carcinoma in Tanzania based on Monte Carlo methods and to evaluate the secondary cancer risks in their lifetime.

Methods: EBRT and HDR-BR were modelled by using the MCNPX Monte Carlo (MC) code. The MC simulations were performed by using validated models and isocentric irradiation of an adult female computational phantom. The organ doses and cancer risks estimates were obtained.

Results: The highest absorbed doses of 6.98×10^{-2} and 5.74×10^{-2} Sv/Gy were recorded in the bladder for BT and EBRT. The higher risk was found for colon at 1.06×10^{-3} in the HDR-BT and 9.75×10^{-5} in the EBRT per 100,000 population at exposure age of 35 years than in the other organs. The risk magnitude decreased with increasing age at exposure. In general, the secondary cancer risks in all sites considered from EBRT and HDR-BR for cervical cancer patient were lower than the baseline risks.

Conclusions: The chances of developing secondary cancer take years following radiation therapy are extremely low, but the results of present study can support to establish a future database on secondary cancer risks involving radiation therapy in patients with cervical cancer by using HDR-BR and EBRT with Co-60 source in Tanzania and other developing countries.

1. Introduction

The risk of radiation-induced secondary cancer after patients with primary cancer undergo radiation treatment has been widely reported by various investigations [1–5]. This is a well-known problem, and related studies have focused on successfully using of new procedures and modalities for treating tumours, such as intensity-modulated x-ray therapy (IMRT) and 3D-conformal radiation therapy (3D-CRT); however, these procedures can potentially increase the risk of secondary cancer [6]. Lee et al. [5] indicated that radiation-induced secondary malignancy of 88.6 per 100,000 population for stomach is obtained after cervical cancer (CxCa) brachytherapy (BT). Qi et al. [7] found the highest secondary cancer risks of 0.0935% and 0.186% in the lungs and lower oesophagus after oesophageal cancer patients underwent IMRT. Radiation treatment aims to provide maximum dose to the tumour target while minimising the radiation dose to the adjacent healthy tissues or organs. Xu et al. [2] stated that the patients' bodies received unavoidably secondary radiation resulting from the leakage in the treatment head and scattered radiation inside the patient's body or from the accelerator components. Organs at risks inevitably receive radiation doses from radiation therapy, and such doses can subsequently increase secondary cancer risks [2,6]. The development of these modern radiation treatment techniques serves to increase patient's lifetimes; however, the related risks of radiation-induced secondary cancer in patients are increased as well [8].

Compared with the previous studies that used modern radiation therapy treatment devices, the current study focuses on traditional technology, that is, the Co-60 source for treating CxCa patients. CxCa is the most common malignancy among the women and has an estimated 485,000 recent cases and approximately 236,000 deaths per year

* Corresponding author at: Department of Engineering and Applied Physics, School of Physical Sciences, University of Science and Technology of China, Hefei, Anhui Province 230027, PR China.
E-mail address: njeketu@mail.ustc.edu.cn (S.A. Suleiman).

https://doi.org/10.1016/j.ejmp.2019.04.024
Received 4 February 2019; Received in revised form 28 March 2019; Accepted 25 April 2019
Available online 04 May 2019

worldwide [9]. As reported, 70% of new cases have occurred in developing countries [10], including Tanzania, which has an estimated of 506 cases per 1,000,000 population [11]. For decades, worldwide largely in developing countries, patients with CxCa have been treated by using high-dose-rate (HDR) BT and external beam radiation treatment (EBRT) involving a Co-60 source [12]. The application of new radiation treatment modalities has a possibility of developing secondary cancers in patients because of the photons and neutrons produced from either inside a patient's body or from a machine head [2]. The application of Monte Carlo (MC) methods to calculate organ dose in computational phantoms has become a worthy alternative [13,14]. In this study, the MC techniques and an adult female computational phantom were used to evaluate organ-absorbed doses from secondary scattered photons outside the target volume. The radiation-induced secondary cancer risks involving the EBRT and HDR-BT Co-60 source have been extensively reported, but organ-absorbed doses outside a target volume remain poorly studied. No MC study has been conducted on secondary cancer risks in patients with CxCa that received treatment involving EBRT and HDR-BT with Co-60 source, which is usually used in Tanzania and in many other developing countries.

This study presents secondary dose calculations in patients with CxCa that underwent EBRT and HDR-BT with Co-60 source by using MC methods. This was achieved by integrating the treatment models and computational adult female phantom into Monte Carlo N-particle eXtended (MCNPX) code. Our aim was to estimate the organ doses and associated lifetime attribute risks (LARs).

2. Materials and methods

2.1. Co-60 HDR source simulation and modelling

In this article, all simulations and the calculations were performed by using the MCNPX MC code [15]. The code has high efficiency in simulating photons, electrons, and neutrons with a wide-ranging energy settings. A photon beam model has been developed for the BEBIG HDR Co-60 source (model Co60.A86) by using the MCNPX methods. The Co-60 source decays through β^- emission, followed by two main γ-photons per disintegration with energies of 1.17 and 1.33 MeV. The two energy spectra of the Co-60 source (i.e. 1.17 and 1.33 MeV) constitute useful radiation for cancer treatment inside the patient's body and are used for source simulations in BT and EBRT. Fig. 1 shows the basic details of a new BEBIG HDR Co-60 source as modelled in our computer simulation. The geometrical modelling and detailed components of the source were obtained from previous studies [16,17]. The Co-60 source was composed of a central cylindrical active core with 3.5 mm length and 0.5 mm diameter. The source core was encased by a 0.15 mm thick cylindrical stainless steel with 1.0 mm outside diameter and a rounded tip that closed the structure. The distal end included a source cable with 5.0 mm length and 0.9 mm diameter.

To obtain the dose rate distributions in water phantom and simulation geometry, the source was placed at the centre of a spherical phantom with a radius of 100 cm, which acted as an unbounded phantom. The density of phantom used was 0.998 g/cm^3, as recommended in the TG-43UI report [18]. The radial dose function, $g_L(r)$, which accounted for dose fall-off along the transverse axis due to the scattered photons and the attenuation in spherical water phantom, was calculated as follows:

$$g_L(r) = \frac{\dot{D}(r, \theta_0)}{\dot{D}(r, \theta_0)} \frac{G_L(r_0, \theta_0)}{G_L(r, \theta_0)} \quad (1)$$

where, $\frac{\dot{D}(r,\theta_0)}{\dot{D}(r_0,\theta_0)}$ is the dose-rate ratio at the distance of interest and the $\frac{G_L(r_0,\theta_0)}{G_L(r,\theta_0)}$ is the geometric functions ratio. In this study, the line-source approximation was used as suggested in the report [18] for the calculation of the geometry function, and was defined as follows:

$$G(r, \theta) = \frac{\beta}{Lr\sin\theta} \text{if} \theta \neq 0^0 \quad (2)$$

$$G(r, \theta) = \left(r^2 - \frac{L^2}{4}\right)^{-1} \text{if} \theta = 0^0 \quad (3)$$

where, L denotes the length of the source core, r is the radial distance, θ and β are angles, in radian. The radial dose function was derived by using the line-source geometry function, with $L = 3.5$ mm over a radial range $r = 0.1$ cm to 20 cm in 0.01 cm steps. The results obtained in the MCNPX code were verified by comparing the calculated $g_L(r)$ with recently published data. Up to 10 million photon histories were simulated and the statistical uncertainty of results was less than 0.1%.

2.2. Co-60 EBRT simulation and photon beam modelling

In this section, different stages of the Co-60 EBRT unit head simulation are presented. A model of the photon beam was developed for Co-60 EBRT by using the MCNPX method. A validated model of telecobalt unit head is also presented in the study [19–21]. Fig. 2 illustrates a simplified model of a teletherapy unit that contains of both fixed and adjustable collimators that define different field size opening to shape the treatment beam and the active material of Co-60 pellets. The pellets of the radioactive source were embedded into the cylindrical capsule made of stainless-steel. On the upper side of the source capsule, the tungsten and lead materials were simulated. All air gaps were included between the material components in this model. To calculate the radiation-scattered doses away from the target tumour, the following two elements should be considered in this model; the leakage photon radiation from the Co-60 treatment head and the scattered photon from the Co-60 treatment head and in the patients' body.

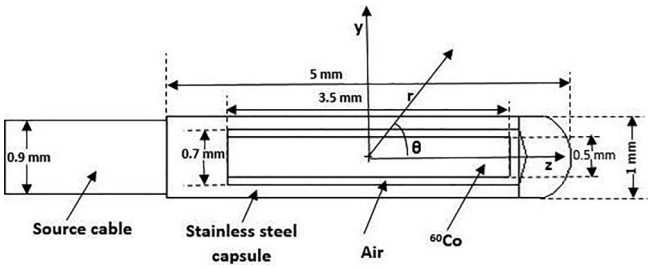

Fig. 1. Internal construction and dimensions of Co-60 HDR source (model Co60.A86) used in the simulations performed in the current work.

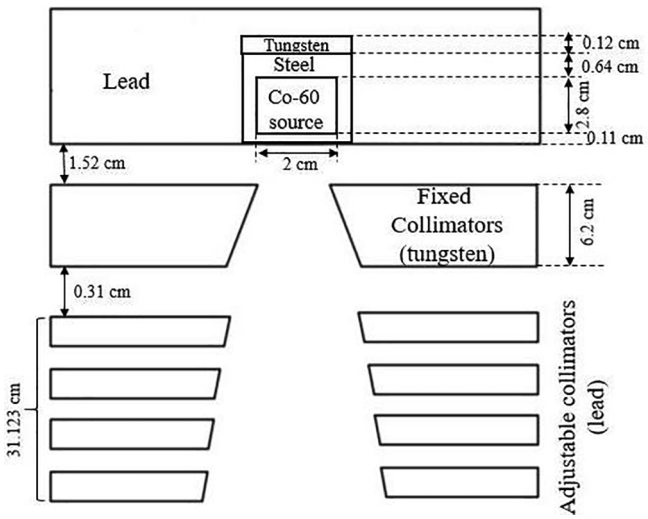

Fig. 2. Schematic representation of Co-60 EBRT unit head model used in the present study.

To validate our model, we used the MCNPX MC code to simulate the water phantom of sizes of 50 cm × 50 cm × 50 cm situated 80 cm below the telecobalt unit head. A spherical cell with 1 cm radius along the central axis of the photon beam was defined in the phantom and was divided into small scoring cells. The energy deposited was calculated in each scoring cell, in the phantom, which was placed at different depths by using the pulse height tally (*F8: p, e card) in MeV units. The ratio in each scoring cell at different depths with maximum dose scoring (i.e. 0.5 cm for Co-60) was used to construct the percentage depth doses (PDDs). The PDDs for the field sizes of 5 cm × 5 cm and 10 cm × 10 cm were calculated and compared with published data in other studies. Moreover, the lateral dose profile was determined in the cross-plane direction with a voxel size of 4 cm × 0.3 cm × 0.6 cm at a depth of maximum dose and 5 cm for a field size of 10 cm × 10 cm. The MCNPX input files were run up to 10^7 histories.

2.3. MC modelling for cervical treatment and equivalent doses calculation

The mesh-based USTC computational phantoms were constructed by using ARCHER MC code [22]. These phantoms were age-dependant (i.e. 5-year-old, 10-year-old, 15-year-old and adult) representing male and female in the different body heights [22–24]. The phantom model, which resembled an adult female that weighed 54 kg (Fig. 3), was used in the current study. To perform organ dose calculations by using the MC techniques, the mesh-based phantoms were converted to voxelized formats with a resolution of 0.2 cm. A spherical cell with a radius 0.75 cm at the precise location of the cervix was defined in the phantom as the target tumour to score the energy per unit mass deposited at the isocentre. An adult female phantom was located below the Co-60 EBRT; thus, a tumour target was located at 80 cm source-to-surface distance (SSD) away from the Co-source. During the radiation treatment, a direct anterior beam with a field size of 10 cm × 10 cm at 80 cm SSD was used to deliver doses to the isocentre per 45 Gy entirely tumour target dose.

Fig. 3. 3D rendering of USTC adult female phantom.

To calculate the equivalent dose by the MCNPX MC code, the pulse height tally (*F8: P, E) was used to scores the deposited energy in the selected organs in terms of MeV. During MC simulation, the results provided by *F8 tally were normalised per source history. The recorded results in MeV were divided by the mass of each organ in kilogram and later times by 1.602×10^{-13} to change the fundamental unit from MeV to J kg^{-1} or Gray (Gy). The total number of photons (N) was defined as follows to achieve 45 Gy-prescribed doses to the entire target volume:

$$N = 45Gy/(D_{tumour/photon}) \tag{4}$$

where, $D_{tumour/photon}$ is the target absorbed dose per photon in MCNPX. The absorbed dose for every critical organ was calculated for an equally weighted field size irradiation giving 45 Gy to the tumour site as follows:

$$D_{critical-organ} = N \times D_{critical-organ/photon} \tag{5}$$

where, $D_{critical\text{-}organ}$ is the total absorbed dose. The cut-off energies of 10 and 500 KeV were set for photon-electron mode. A 24-core MC computer server with 2.6 GHz RAM running on Ubuntu operating system was used. An average time of ~11.2 CPU-hours was required for each MC simulation to obtain a statistically reliable error of less than 1% for each organ. Because we simulate the photon in the MC code, the radiation weighting factor (w_R) of 1 was used to obtained the radiation equivalent dose in every organs considered. The total number of histories up to 30 million particles were simulated.

Moreover, the BT treatment was modelled with MCNPX by using an adult female phantom and the exact geometry of the HDR Co-60 source (Fig. 1). The length and diameter of Co-60 source were 3.5 and 0.5 mm. The treatment involving a single dwell position in the centre of the sphere used in clinical plans was considered in this study. In the MC calculations, the energy distribution was scored in the selected organs by using the *F8 tally of the MCNPX. This tally recorded the energy in MeV, which was then converted into absorbed dose. The results of this paper involving an adult female computational phantom may not be generalisable into all females. However, the data values of organ dose distribution presented in this study are expected to be typical of a broad range of clinical situations. Several particle histories were run to ensure that the statistical uncertainty of the MC results were less than 1% for most organs.

2.4. Cancer incidence risk evaluation attributable to secondary doses

Cancer incidence risks to organs due to scattered photons from HDR Co-60 BT and Co-60 EBRT were estimated by using the biological effects of ionising radiation (BEIR) VII methods [25,26]. The methodology for calculating secondary cancer risks can be found inside the BEIR VII report, Chapter 12. This report developed models for excess absolute risk (EAR) and excess relative risk (ERR), which depend on the total dose equivalent D, sex of cancer patient s, age at treatment e in years and the total time since treatment a in years. The EAR and ERR of secondary cancer were computed by using the following equation:

$$ERR(D, s, e, a) and EAR(D, s, e, a) = D \bullet \beta_s \bullet exp(\gamma e^*)\left(\frac{a}{60}\right)^{\eta} \tag{6}$$

where, e^* is $(e - 30)/10$ when the value of e is less than 30 years and zero when the value of $e \geq 30$ years. γ, β_s and η represent the model parameters which are offered for ERR and EAR in the BEIR VII [25]. For solid cancer sites, the ERR and EAR are linear functions of dose equivalence. The risk models are used to link the gap between the cancer induction risk and the equivalent doses. Using the risk model values, the lifetime attributable risk (LARs) for a secondary cancer incidence was calculated as follows [25,26]:

$$LAR(D, e) = \int_{e+L}^{a_{max}} (ERR \bullet \lambda_1^c \bullet S(a)/S(e)da)^{0.7} \times \int_{e+L}^{a_{max}} (EAR \bullet S(a)/S(e)da)^{0.3} \quad (7)$$

where, L is the latency period after exposure (for solid tumour is 5 y), $\lambda_I^C$is baseline risk for an exposed individual and $S(a)/S(e)$ is the possibility of a cancer patient surviving from age e to age a founded on the data existing at the National Bureau of Statistics in Tanzania [27]. Following the recommendation of BEIR VII report, the weights for EAR and ERR integrals were described as 0.3 and 0.7, for most organs. For the lung cancer risk, the weights for the models in Eq. (7) were reversed, that is, 0.3 used for ERR estimate and 0.7 for the EAR estimate; only the EAR model was recommended for breast cancer [28]. No EAR model was observed for thyroid cancer risk, and LAR was estimated by using only the ERR model. For the final total risk estimation, the weighted average of LAR used the values of EAR and ERR risk models divided by dose and dose-rate effectiveness factor of 1.5 as recommended by the BEIR report [26]. Based on the present life expectancy at birth of a Tanzanian female aged 63.8 years, we set the ages at exposure between 35 and 50 years with five-year increments and the attained age at 60 years.

3. Results

3.1. Validation of the simulated models

Fig. 4 shows the g (r) for the HDR Co-60 source compared with published results. For the HDR Co-60 source, the maximum percentage difference between the g (r) results and the data by Granero et al. [16] were 1.14%, 1.59%, 1.17% and 2.78% at 10, 12, 15 and 20 cm, respectively. However, in the MC results, the statistical uncertainties for all points were less than 0.1%, which were within the final uncertainty obtained by Granero et al. [16] who found it to be less than 0.7%. The results in Fig. 4 depict that our isotropic cylindrical model for the HDR Co-60 source was suitable for this study.

Fig. 5 depicts the comparison plots of PDDs between the EBRT Co-60 source and the data published in the BJR Suppl 25 at field sizes of 10 cm × 10 cm and 5 cm × 5 cm. For all calculations, the field sizes were taken at the point of maximum dose (i.e. 0.5 cm for Co-60 source) beneath the surface of simulated water phantom. A comparative plot revealed that there is a good agreement between the MC calculation results and that published in BJR Suppl. 25. Significantly deviations below 0.5% were detected between the calculated and published data,

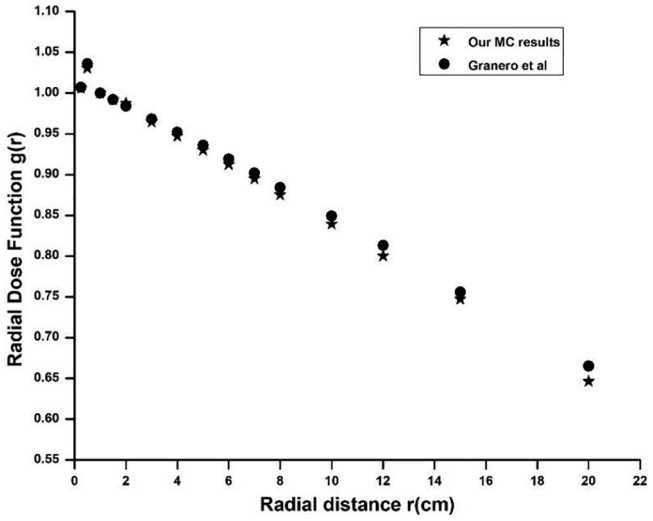

Fig. 4. Plotted MC results of radial dose function against radial distance for the BEBIG Co-60 (model Co0.A86) source compared with data published by Granero et al.

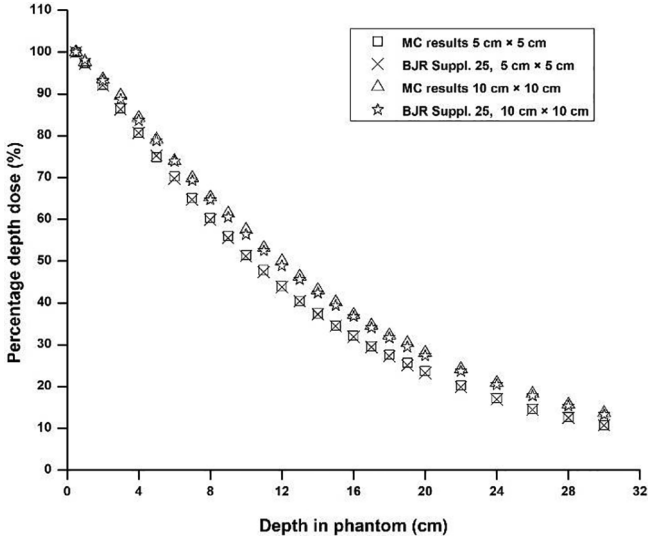

Fig. 5. Plotted percentage depth dose versus depth in phantom obtained from MC calculation compared with data published in the BJR Suppl. 25 for field sizes of 10 × 10 and 5 × 5 cm^2.

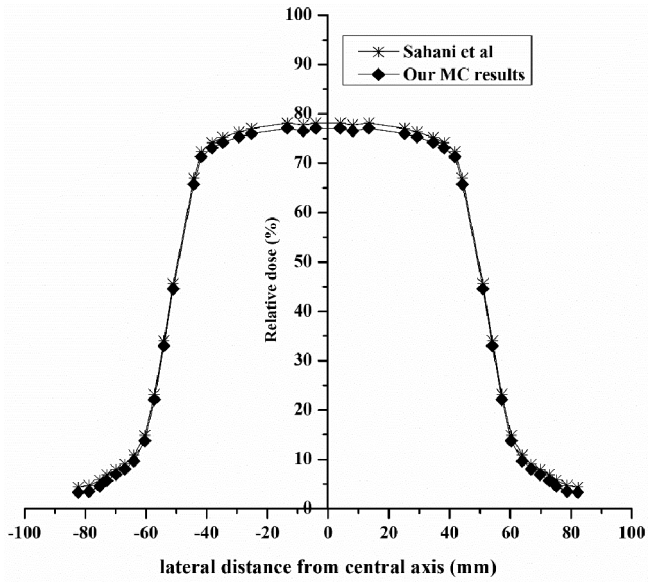

Fig. 6. Comparison of the beam profile from MC simulation at maximum dose and depths of 5 cm in a water phantom and data from Sahani et al. for a filed size of 10 × 10 cm$^{2.}$

and the maximum was close to 1.5%. The lateral beam profile was determined at the maximum dose and 5 cm depth for a field size of 10 × 10 cm^2. A comparison plot of our MC results and experimentally measured beam profiles obtained by Sahan et al [29] is shown in Fig. 6. Good agreement was attained between the two sets of data, whereby statistical uncertainties of the MC simulation results were below 0.1%. Consequently, the results confirm that the geometrical dimensions for our model were accurately considered in the MC simulations.

3.2. Equivalent doses in various organs away from tumour target

The comparison between the photon absorbed doses to various organs in the patients with CxCa during HDR-BT and EBRT involving Co-60 source is provided in Table 1. The results in Table 1 were normalised to the maximum prescribed dose to the target tumour and expressed in Sievert per prescribed Gray (Sv/Gy). In the case of BT, inverse square

Table 1
Comparison of the absorbed doses (Sv/Gy) to various organs in the patients with CxCa.

Organ	HDR Co-60 BT	EBRT Co-60
Colon	6.11×10^{-3}	2.99×10^{-4}
Lungs	1.99×10^{-4}	5.21×10^{-6}
Stomach	6.80×10^{-4}	2.29×10^{-5}
Ovaries	1.98×10^{-2}	1.40×10^{-3}
Bladder	6.98×10^{-2}	5.74×10^{-2}
Oesophagus	5.79×10^{-5}	1.28×10^{-6}
Liver	7.07×10^{-4}	2.26×10^{-5}
Thyroid glands	2.92×10^{-5}	4.82×10^{-7}
Brain	7.25×10^{-6}	1.05×10^{-7}
Salivary glands	1.39×10^{-5}	2.04×10^{-7}
Adrenals	5.89×10^{-4}	2.05×10^{-5}
Gall bladder	6.62×10^{-4}	2.07×10^{-5}
Small intestine	6.00×10^{-3}	3.85×10^{-4}
Kidneys	1.40×10^{-3}	5.92×10^{-4}
Pancreas	1.16×10^{-3}	4.33×10^{-5}
Spleen	6.80×10^{-4}	2.29×10^{-5}
Thymus	7.00×10^{-5}	1.30×10^{-6}
Heart wall	1.74×10^{-4}	4.34×10^{-6}
Breasts	1.07×10^{-4}	1.83×10^{-6}

law is the most dominant physical result, whereby the radiation dose varies inversely as the square of the distance from the radioactive source. Practically, this allows for excessive radiation dose to the target tumour with relatively low radiation dose to the organs far away from the target, as shown in Table 1. The higher radiation doses in EBRT were the most dominant from the telecobalt machine leakage and radiation scattering from the machine or inside the patient's body [2]. For the selected organs, the normalised organ absorbed doses were higher in HDR-BT than in the EBRT, because the distance between radioactive source and normal organs in HDR-BT was shorter compared with EBRT. The short distance caused the increased radiation exposure and organ-absorbed doses. The larger absorbed doses were calculated in the bladder, ovaries and colon in both treatment modalities (Table 1). Similarly, for the brain and other organs away from the target volume, the absorbed doses decreased to 7.25×10^{-6} and 1.05×10^{-7} Gy for the HDR-BT and EBRT, respectively.

3.3. Estimate of second cancer risk

Table 2 presents the comparison results of the LARs associated with HDR-BT and EBRT for some organs away from the target tumour

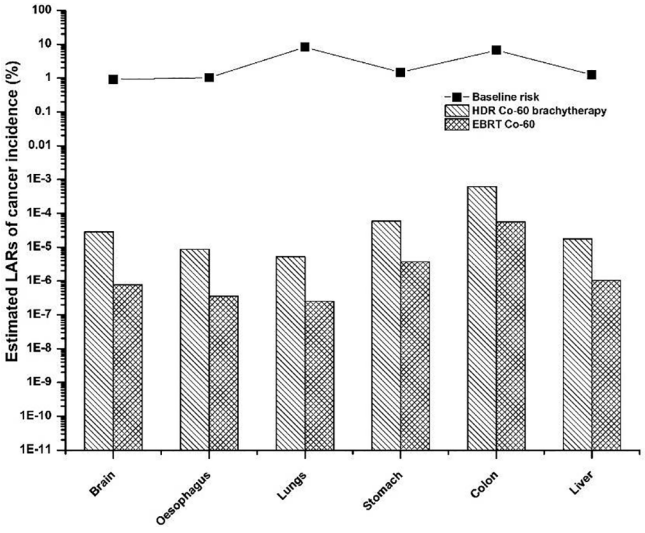

Fig. 7a. Comparison of LARs of different anatomical sites distant from the target volume for an adult patient with cervical exposed at 50-year-old and the attained age of 60 years.

depending on age at exposure. Several important conclusions can be drawn from Table 2. For all of the considered organs, the LAR values denote the function of age at exposure and demonstrate a general feature of the BEIR-VII risk model. By designating the age of exposure of cancer patient as 50-years as a reference value, we found that the highest value of LAR per 100,000 in the population was in the colon (i.e. 6.11×10^{-4} and 5.50×10^{-5} for the HDR-BT and EBRT, respectively). The relatively lowest LAR was observed in the lungs (i.e. 5.15×10^{-6} and 2.52×10^{-7} for the HDR-BT and EBRT, respectively). Fig. 7a and 7b present the results of LARs of the different anatomical sites of an adult female patient exposed at 50 years of age compared with the values of baseline risk obtained to the SEER Cancer Statistics Review [30].

Another risk model was proposed by the NCRP report 116 to calculate secondary cancer risk [31]. In this model, the risk value coefficients were primarily based on the cancer incidence data from a Japanese atomic-bombing survivor. However, the NCRP model considered all of the age groups and entered the populations, thus making it relatively more diverse than the BEIR VII model. The risk estimates for each organ site selected were determined by multiplying

Table 2
Comparison of LAR for various organs in accordance with age at exposure to HDR-BT and EBRT with Co-60 source (per 100,000 population) by using the BEIR-VII model.

		Age at Exposure (yrs)			
	Organs	35	40	45	50
HDR BT	Stomach	1.02×10^{-4}	1.00×10^{-4}	8.75×10^{-5}	5.86×10^{-5}
	Colon	1.06×10^{-3}	$1.05 \times 10^{--3}$	9.12×10^{-4}	6.11×10^{-4}
	Liver	3.05×10^{-5}	3.00×10^{-5}	2.62×10^{-5}	1.75×10^{-5}
	Oesophagus	1.50×10^{-5}	1.47×10^{-5}	1.29×10^{-5}	8.61×10^{-6}
	Kidneys	2.04×10^{-5}	2.01×10^{-5}	1.75×10^{-5}	1.17×10^{-5}
	Brain	4.93×10^{-5}	4.85×10^{-5}	4.22×10^{-5}	2.83×10^{-5}
	Lungs	8.96×10^{-6}	8.81×10^{-6}	7.68×10^{-6}	5.15×10^{-6}
	Breasts	8.43×10^{-5}	8.28×10^{-5}	7.22×10^{-5}	4.84×10^{-5}
EBRT	Stomach	6.46×10^{-6}	6.35×10^{-6}	5.54×10^{-6}	3.71×10^{-6}
	Colon	9.75×10^{-5}	9.59×10^{-5}	8.36×10^{-5}	5.60×10^{-5}
	Liver	1.83×10^{-6}	1.80×10^{-6}	1.57×10^{-6}	1.05×10^{-6}
	Oesophagus	6.21×10^{-7}	6.10×10^{-7}	5.32×10^{-7}	3.57×10^{-7}
	Kidneys	1.62×10^{-6}	1.59×10^{-6}	1.39×10^{-6}	9.28×10^{-7}
	Brain	1.34×10^{-6}	1.31×10^{-6}	1.15×10^{-6}	7.67×10^{-7}
	Lungs	4.39×10^{-7}	4.32×10^{-7}	3.76×10^{-7}	2.52×10^{-7}
	Breasts	8.43×10^{-5}	8.28×10^{-5}	7.22×10^{-5}	4.85×10^{-5}

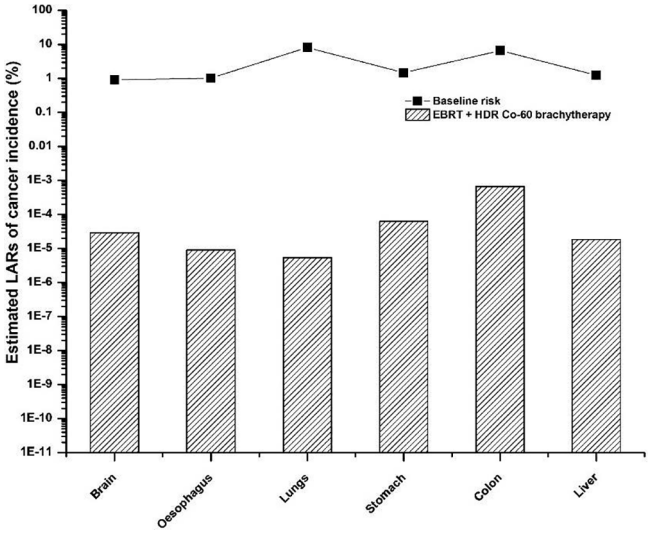

Fig. 7b. Comparison of LARs of different anatomical sites distant from the target volume for an adult patient with a combination of Co-60 EBRT and Co-60 BT of cervical exposed at 50-year old and the attained age of 60 years.

Table 3
Risk of secondary cancer for various organs (%) using the NCRP model.

Organs	HDR Co-60 BT	EBRT Co-60
Stomach	9.80×10^{-3}	6.20×10^{-4}
Colon	8.80×10^{-2}	8.06×10^{-3}
Liver	3.39×10^{-3}	2.04×10^{-4}
Oesophagus	2.78×10^{-4}	1.15×10^{-5}
Kidneys	2.02×10^{-2}	1.60×10^{-3}
Brain	8.70×10^{-6}	2.36×10^{-7}
Lungs	2.87×10^{-3}	1.41×10^{-4}
Breasts	1.54×10^{-3}	4.94×10^{-5}

the whole-body equivalent-dose coefficient of 5% per Sv [31]. The maximum absolute risks of fatal cancer for various organs attributable to secondary radiation in the NCRP model are presented in Table 3. The results in the NCRP model were considerably higher compared with those in the BEIR VII risk model.

4. Discussion

4.1. Equivalent doses in various organs away from target tumour

In the present study, an adult female phantom was used to calculate the absorbed doses in organs at risk and later was used to estimate the secondary cancer risks related to CxCa irradiations. The BT and EBRT involving Co-60 source were used for patient's irradiations with CxCa. As seen in Table. 1, those organs extremely close to or within the target volume have relatively high radiation doses which decline as the distance from the treatment volume increases. BT is related to various side effects because it delivers high doses into a target. However, the doses to some organs are influenced by the attenuation of photon beams. In EBRT, the doses to distant organs are mainly caused by the scattered photons from the treatment head [2], suggesting that only a significant fraction of the total amount of radiation doses could reach non-target organs. The absorbed organ doses in patients with CxCa are higher in BT than in EBRT. In both treatment modalities, the absorbed organ doses were are higher in the bladder, ovaries, and colon than in other organs. Compared with colon, doses to the bladder were 6.4% higher for BT and 5.7% higher for EBRT. The observed difference in the results could be attributed to the differences in radiation photon exposure between the considered treatment modalities. For distant organs, such as brain and salivary glands, the absorbed doses were nearly zero and decreased by 99.9% with respect to the absorbed doses to the bladder in both BT and EBRT, respectively. Irradiation of distant organs during BT involves the impact of attenuation of high-energy photons passing inside the patient's body, whereas in EBRT generally involves photon radiation scattered within treatment head and inside the human body [2]. Zaman et al. [32] performed a comparative study and revealed that the rectum obtains the highest doses during HDR Co-60 BT of the patients with CxCa. In the planning study of Yong et al. [33] on the dosimetric impact of applicator displacement during the HDR Co-60 BR of CxCa, the maximum photon doses of rectum and bladder were also found in 2 cc of the organ (D_{2cc}) using the HDR Co-60 BT for cervical cancer. Our results demonstrated that the organs closest to the tumour target, such as bladder and colon, received relatively high absorbed doses.

The use of HDR Co-60 (1.25 MeV) source is comparable to the Yb-169 (92.7 keV) and Ir-192 (280 keV) sources. The average energy of Yb-169 source is less than that of the Co-60 and Ir-192 sources; this led the photon interaction inside the medium to be dominant by multiple radiation scattering for higher photoelectric absorption [17]. Venselaar et al. [34] showed that outside of the target volume, the dose comparisons in the peripheral organs at risks show a reverse behaviour (Co-60 doses < Ir-192 doses) at short distances, as when the distance increases from the target volume (Co-60 doses > Ir-192 doses). The Co-60 source has advantages over Ir-192 and Yb-169 due to its lower energy photons, higher dose rate constant and longer half-life. These properties make the Co-60 source suitable for use in BT application in many developing countries, although a proper shielding is required for the source.

4.2. Secondary cancer risks

In this study, the highest LARs per 100,000 of the population from CxCa patients were found in the colon, and lower values were in the lungs for both BR and EBRT. The LAR values for selected organs of CxCa patients in the BR treatment were higher than in the EBRT in all ages at exposure as shown in Table 2. By contrast, the organs close to the target volume have higher LARs but have considerably lower values than the baseline risks (Fig. 7a), showing that the secondary cancer risks were lower in a patient who received BT and EBRT for CxCa. Moreover, the risk values for the combination of two modalities (i.e. EBRT and HDR-BT) were also lower than the baseline risks (Fig. 7b) but higher when separate treatment was considered. Compared with Fig. 7a, the risk values in the colon (Fig. 7b) were 5.6×10^{-3} and 6.11×10^{-2}% higher than the BT and EBRT. In Table. 2 results show that the different ages at exposure and the LAR values have a reverse relationship because the body tissue of younger aged patients is more sensitive to the effects of radiation. The risk of secondary cancer was also found in the Table. 3 for various organs using the NCRP model. In both treatments (i.e. HDR-BT and EBRT), the highest risk was in the colon, and the relatively lowest was in the brain. In comparison with the colon, the risk values in the brain were reduced by 99.9% in BT and EBRT, respectively.

The risks evaluation after radiation treatment of CxCa is significant for clinical investigation, but few studies are available for comparison with the current study. And the secondary cancer is conceptually different when various risk models are used. The BEIR VII report depended on the age-specific risk model, site-specific cancers and was chosen in the literature. The BEIR VII report may provide a more reliable estimate of cancer risk than the NCRP model [25]. In this manner, this study was based on the use of Tanzanian population data and the BEIR VII risk model. As expected, the organs closest to the irradiation isocentre had the highest LARs, but their values were substantially lower than the baseline risks.

5. Conclusion

This research was conducted to calculate non-target organ absorbed doses and related risks for cancer in Tanzania from scattered photons in

cervical radiation treatment involving Co-60 source. The MC simulations involved detailed use of EBRT and HDR-BT Co-60 source models. The USTC-adult female phantom was used to estimate the absorbed doses in each organ at risk. The organs located close to the target tumour had the highest absorbed doses; however, the doses decreased with increasing distance from the target. In general, the LAR values of cancer incidence in all considered anatomical sites were lower than the baseline risks. A follow-up study should be conducted to establish a future database on secondary cancer risks involving radiation treatment in patients with cervical carcinoma to provide useful records when patients with cancer undergo radiation therapy more than once.

Acknowledgments

The authors would like to thank the members of the Center of Radiological Medical Physics team at USTC for their helpful advice on the article and great assistance in running the MC MCNPX code. Mr. Suleiman A. Suleiman is gratefully acknowledged to the CAS-TWAS President's Fellowship Programme for the grant awarded to pursue full-time Ph.D. programme at the University of Science and Technology of China.

Funding

This research was financially supported by the National Key R&D Program of China (Grant No. 2017YFC0107504) and the Natural Science Foundation of China (Grant Nos. 11375182).

References

[1] Kry SF, Bednarz B, Howell RM, Dauer L, Followill D, Klein E, et al. AAPM TG 158: Measurement and calculations of doses outside the treatment volume from external-beam radiation therapy. Med Phys 2017;44:e391–429.
[2] Xu XG, Bednarz B, Paganetti H. A review of dosimetry studies on external-beam radiation treatment with respect to secondary cancer induction. Phys. Med. Biol. 2008;53:R193–241.
[3] Travis LB, et al. Second Primary Cancers and Cardivascular Disease after Radiation Therapy. NCRP Report No. 170. Bethesda, Maryland. 2011.
[4] Brenner DJ, Curtis RE, Hall EJ, Ron E. Second malignancies in prostate carcinoma patients after radiotherapy compared with surgery. Cancer 2000;88:398–406.
[5] Lee B, Ahn SH, Kim H, Son J, Sung J, Han Y, et al. Secondary cancer-incidence risk estimates for external radiotherapy and high–dose-rate BT in cervical cancer: phantom study. J. Appl. Clin. Med. Phys. 2016;17:124–32.
[6] Hall EJ, Wuu CS. Radiation-induced second cancers: the impact of 3D-CRT and IMRT. Int. J. Radiat. Oncol. Biol. Phys. 2003;56:83–8.
[7] Qi Y, He L, Wang Z, Liu Y, Liu H, Huo W, et al. Evaluation of secondary dose and cancer risk for out-of-field organ in esophageal cancer IMRT in a Chinese hospital using Atom Phantom measurements. Radiat. Prot. Dosim. 2017;177. 398 396.
[8] D'Errico F. Dosimetric issues in radiation protection of radiotherapy patients. Radiat. Prot. Dosim. 2006;118:205–12.
[9] Fitzmaurice C, Dicker D, Pain A, Hamavid H, Moradi-Lakeh M, MacIntyre MF, et al. The global burden of cancer 2013. JAMA Oncol. 2015;1:505–27.
[10] International Agency for Research on Cancer (IARC). Latest world cancer statistics Global cancer burden rises to 14.1 million new cases in 2012: marked increase in breast cancers must be addressed. Available on. < http://www.iarc.fr/en/media-centre/pr/2013/pdfs/pr223_E.pdf > .
[11] GLOBOCAN 2012: Estimated cancer incidence, mortality and Prevalence Worldwide in 2012. Available on. < http://globocan.iarc.fr > .
[12] Garipagaogle M, Tuncel N, Dalmaz M, Gulkesen H, Toy A, Kizildag AU, et al. Changes in applicator positions and dose distribution between high dose BT fractions in cervical carcinoma patients receiving definitive radiotherapy. Br J Radiol. 2006;79. 509 509.
[13] Bednarz B, Monte XuXG. Carlo Modeling of a 6 and 18 MV Varian Clinical Medical Accelerator for in-field and out-of-field Dose Calculations: development and validation. Phys. Med. Biol. 2009;54:pp.N43-N57.
[14] Barquero R, Edwards TM, Inigues MP, Vega-Carrillo HR. Monte Carlo simulation estimates of neutron doses to critical organs of a patient undergoing 18 MV x-ray LINAC-based radiotherapy. Med. Phy. 2005;32:3579–88.
[15] Pelowits DB. MCNPX User's Manual Version 2.7.0. LA-CP-11-00438. 2011.
[16] Granero D, Perez-Calatayud J. Technical note: dosimetric study of a new Co-60 source used in BT. Med. Phys. 2007;34:3485–8.
[17] Safigholi H, Han DY, Mashouf S, Soliman A, Meigooni AS, Owrangi A, et al. Direction modulated brachytherapy (DMBT) for treatment of cervical cancer: a planning study with ^{192}Ir, ^{60}Co and ^{169}Yb HDR sources. Med Phys 2017;12:6538–47.
[18] Rivard MJ, CourseyBM Hanson WF, Huq MS, Ibbott GS, Mitch MG, Nath R, et al. Upadate of AAPM task Group No. 43 Report: a revised AAPM protocol for BT dose calculations. Med. Phys. 2004;31:633–74.
[19] Miro R, Juste B, Gallorado S, Santos A, Verdu G. Cobalt therapy dosimetric calculations over a voxelized heterogeneous phantom: validation of different monte carlo models and methodologies against experimental data. IEEE Trans Nucl Sci 2006;53:3808–17.
[20] Sichuan BT, Sohrabpour M. Monte Carlo dose calculations for radiotherapy machines: theratron 780-C teletherapy case study. Phy. Med. Biol. 2004;49:807–18.
[21] Suleiman SA, Qi Y, Xu XG. Monte Carlo Simulation of out-of-field organ doses and cancer risk in Tanzania for radiation therapy of unilateral retinoblastoma using a ^{60}Co unit. Radiat. Prot. Dosim. 2018;179:263–70.
[22] Pi Y, Liu T, Xu XG. Development of a set of Mesh-based and age-dependant Chinese phantoms and application for CT dose calculations. Radiat. Prot. Dosim. 2018;179:370–82.
[23] Pi Y, Zhang L, Huo W, Feng M, Chen Z, Xu XG. Development and application of set of mesh-based and age-dependent Chinese family phantoms for radiation protection dosimetry: preliminary data for external photons beams. 13th International Conference on Radiation Shielding & 19th Topical Meeting of the Radiation Protection & Shielding Division of the ANS (ICRS13-RPSD2016). 2016.
[24] Pi Y, Feng M, Huo W, Zhang L, Liu T, Lin H, Yang L, Zheng F, Tan H, Pan F, Chen Z, Xu XG. Development of mesh-based age-dependent family phantoms. 5th International Workshop on Computational Human Phantoms (CP2015), Seoul, Korea, July. 2015.
[25] Bednarz B, Athar B, Xu XG. A comparative study on the risk of second primary cancers in out-of-field organs associated with radiotherapy of localized prostate carcinoma using Monte Carlo-based accelerator and patient models. Med. Phys. 2010;37:1987–94.
[26] BEIR, Health Risks from Exposure to Low Levels of Ionizing Radiation: BEIR VII, Phase 2. Washington, DC: The National Academy of Sciences; 2006.
[27] Tanzania National Bureau of Statistics. Available on. < http://www.nbs.go.tz/ > .
[28] Preston DL, Mattsson A, Hilmberg E, Shore R, Hildreth NG, Boice JD. Radiation effects on breast cancer risk: a pooled analysis of eight cohorts. Radiat Res. 2002;158:220–35.
[29] Sahani G, et al. Monte Carlo simulation based study of a proposed multileaf collimator for a telecobalt machine. Med. Phys. 2013;40:21705–16.
[30] National Cancer Institute. SEER Cancer Statistics Review. Available on. < http://seer.cancer.gov/csr/1975 2014 > .
[31] National Council on Radiation Protection and Measurements. Limitation of exposure to ionizing radiation. NCRP Report 116. Bethesda (MD): National Council on Radiation Protection and Measurements1993.
[32] Zaman ZK, Ung NM, Malik RA, Ho GF, Phua VCA, Jamalludin Z. Comparison of planned and measured rectal dose in-vivo during high dose rate cobalt-60 brachytherapy of cervical cancer. Med. Phys. 2014;30:980–4.
[33] Yong JS, Ung NM, Jamalludin Z, Malik RA, Wong JH, Liew YM, et al. Dosimetry impact of applicator displacement during high dose rate (HDR) Cobalt-60 brachytherapy for cervical cancer: A planning study. Radiat. Phys. Chem. 2016;119:264–71.
[34] Venselaar JL, Van der Giessen PH, Dries WJ. Measuremets and calculation of the dose at large distances form brachytherapy sources: Cs-137, Ir-192 and Co-60. Med. Phys. 1996;24:537–43.